

## Article

# Improvement in the Environmental Stability of Haloalkane Dehalogenase with Self-Assembly Directed Nano-Hybrid with Iron Phosphate

Jianxiong Chen <sup>1,2,†</sup>, Xiaodong Ming <sup>1,2,†</sup>, Zitao Guo <sup>1,2</sup>, Yi Shi <sup>1,2</sup> , Moying Li <sup>1,2</sup>, Zhongpeng Guo <sup>1,2</sup>, Yu Xin <sup>1,2</sup> , Zhenghua Gu <sup>1,2</sup>, Liang Zhang <sup>1,2,\*</sup>  and Xuan Guo <sup>3,\*</sup>

<sup>1</sup> National Engineering Research Center of Cereal Fermentation and Food Biomanufacturing, Jiangnan University, Wuxi 214122, China; cjx1274777@163.com (J.C.); mx69327@163.com (X.M.); guozt@jiangnan.edu.cn (Z.G.); shiyi0621@jiangnan.edu.cn (Y.S.); wuweisong2009@126.com (M.L.); zgao@insa-toulouse.fr (Z.G.); yuxin@jiangnan.edu.cn (Y.X.); guzhenghua2011@163.com (Z.G.)

<sup>2</sup> Jiangsu Provincial Research Center for Bioactive Product Processing Technology, Jiangnan University, Wuxi 214122, China

<sup>3</sup> State Key Laboratory of NBC Protection for Civilian, Research Institute of Chemical Defense, Academy of Military Science, Beijing 102205, China

\* Correspondence: zhangl@jiangnan.edu.cn (L.Z.); xuan.guo@siat.ac.cn (X.G.)

† These authors contributed equally to this work.

**Abstract:** Haloalkane dehalogenase (DhaA) catalyzes the hydrolysis of halogenated compounds through the cleavage of carbon halogen bonds. However, the low activity, poor environmental stability, and difficult recycling of free DhaA greatly increases the economic cost of practical application. Inspired by the organic–inorganic hybrid system, an iron-based hybrid nanocomposite biocatalyst FeHN@DhaA is successfully constructed to enhance its environmental tolerability. A series of characterization methods demonstrate that the synthesized enzyme–metal iron complexes exhibit granular nanostructures with good crystallinity. Under optimized conditions, the activity recovery and the effective encapsulation yield of FeHN@DhaA are 138.54% and 87.21%, respectively. Moreover, it not only exhibits excellent immobilized enzymatic properties but also reveals better tolerance to extreme acid, and is alkali compared with the free DhaA. In addition, the immobilized enzyme FeHN@DhaA can be easily recovered and has a satisfactory reusability, retaining 57.8% of relative activity after five reaction cycles. The results of this study might present an alternative immobilized DhaA-based clean biotechnology for the decontamination of organochlorine pollutants.

**Keywords:** haloalkane dehalogenase; immobilization; organic–inorganic hybrid system; catalytic activity; decontamination



**Citation:** Chen, J.; Ming, X.; Guo, Z.; Shi, Y.; Li, M.; Guo, Z.; Xin, Y.; Gu, Z.; Zhang, L.; Guo, X. Improvement in the Environmental Stability of Haloalkane Dehalogenase with Self-Assembly Directed Nano-Hybrid with Iron Phosphate. *Catalysts* **2022**, *12*, 825. <https://doi.org/10.3390/catal12080825>

Academic Editor: Aniello Costantini

Received: 28 June 2022

Accepted: 25 July 2022

Published: 27 July 2022

**Publisher's Note:** MDPI stays neutral with regard to jurisdictional claims in published maps and institutional affiliations.



**Copyright:** © 2022 by the authors. Licensee MDPI, Basel, Switzerland. This article is an open access article distributed under the terms and conditions of the Creative Commons Attribution (CC BY) license (<https://creativecommons.org/licenses/by/4.0/>).

## 1. Introduction

Haloalkane dehalogenase (EC3.8.1.5 DhaA) is a kind of hydrolytic enzyme which can catalyze the cleavage of carbon–halogen bonds in halogenated compounds [1]. DhaA was first found in autotrophic *Flavobacterium* GJ10 [2]. Since then, it has been excavated in marine bacteria, pathogens and archaea [3,4]. Haloalkane dehalogenase has attracted much attention because of its unique catalytic mechanism and extensive substrate specificity, which not only has important theoretical value, but also has crucial biotechnology and environmental significance in practice [5,6]. At present, it has been used in the recovery of by-products from chemical processes [7], the bioremediation of toxic environmental pollutants [8], the decontamination of chemical warfare agents [9], as a biosensor for environmental pollutants [10], and for protein labeling and cell imaging for protein analysis [11]. However, its large-scale applications are limited due to low catalytic activity, sensitivity to environmental factors, and poor reusability [12].

In recent years, the immobilization of DhaA on some support materials, such as epoxy resin ES-103B [13], meso-cellular foam [14], arabinogalactan [15], inulin [16], mesoporous silica [17], and A502Ps resin [18], has provided a general approach to improve the stability of the DhaA. However, the relative activity of these immobilized enzymes is lower than that of free enzymes, mainly due to the mass transfer limitation and conformational change [17]. The same phenomenon is also common in other traditional immobilization techniques [19,20]. Therefore, it is a priority to develop new enzyme immobilization materials and techniques with higher catalytic activity and stability.

In the third millennium, researchers used a series of new nanostructured materials as enzyme carriers to solve the problem of enzyme activity [21]. Recently, Ge et al. reported a mild and direct co-precipitation approach to obtain a hybrid nanomaterial with interesting flower-like structures [22]. This fascinating nanocomposite structure can be simply synthesized by adding proteins to the metal ion solution, which has attracted considerable research attention. The synthesis process is environmentally friendly and has no toxic by-products. In addition, hybrid nanoflowers have a high surface area–volume ratio, which reduces the mass transfer limitation among enzymes, substrates and products [23,24]. Most importantly, compared with free enzymes, hybrid nanoflowers have higher activity, better stability, good reusability and great application potential [25]. The superior catalytic performance of hybrid nanoflowers means that they have widespread application, with distinct operational fields including industrial biocatalysts, biomedical, and environmental bioremediation [26]. For example, the lipase-Cu<sub>3</sub>(PO<sub>4</sub>)<sub>2</sub> hybrid nanoflower has been applied to the synthesis of biodiesel efficiently [27], the DNA hybrid nanoflower has been applied for single-excitation multiplexed imaging and traceable targeted drug delivery [28], and laccase-Cu<sub>3</sub>(PO<sub>4</sub>)<sub>2</sub> hybrid nanoflowers have been applied for decolorizing dyes in wastewater [29].

Despite the progressive nature of the immobilization approach, the immobilization of DhaA by self-assembly coprecipitation has not been studied before. In this study, a variety of inorganic components are designed to synthesize DhaA inorganic hybrid nanocomposites and the preparation process is further optimized. The synthesized hybrid nanocomposites are characterized by field-emission scanning electron microscopy (FE-SEM, JSM-7800F, Tokyo, Japan), an X-ray diffractometer (XRD, D2 PHASER, Brook AXS Ltd., Berlin, Germany) and Fourier transform infrared spectroscopy (FT-IR, Thermo Scientific Nicolet iS5, Waltham, MA, USA). In addition, the stability and catalytic activity of immobilized enzymes are also studied to explore their potential in practical application. This study provides a new proof of concept for improving the activity of immobilized DhaA.

## 2. Results and Discussion

### 2.1. Expression and Purification of DhaA

*E. coli* BL21 (DE3) cells which were transformed with the recombinant plasmid pET28a-DhaA exhibited a high expression level of recombinant proteins. As shown in Figure 1, an obvious accumulation of the expressed protein band was observed at about 37 kDa through 10% SDS-PAGE analysis, which was consistent with the predicted relative molecular weight. Lane 3 in the gel showed a clear target protein band, indicating that a relatively pure DhaA was obtained, which was beneficial to our next immobilization study.

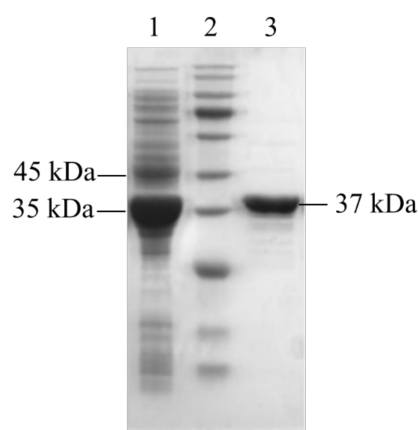


**Figure 1.** SDS-PAGE profiling of DhaA. Lane 1: crude lysate; Lane 2: marker; Lane 3: purified DhaA (37 kDa).

## 2.2. Preparation of Metal-DhaA Hybrid Nanocomposites

As we know, the properties and morphology of hybrid nanoflowers are affected by many factors, including metal ions, enzyme concentration, pH value, buffer concentration, and incubation time [23,24]. In order to find out the best dynamics of immobilized DhaA, the above preparation conditions were optimized.

### 2.2.1. The Effects of Metal Ions

In general, hybrid nanoflowers prepared by self-assembly co-precipitation can greatly increase the enzyme activity of metal enzymes, such as laccase [30], horseradish peroxidase [31], amylase [32], urease [33], and organophosphorus hydrolase [34]. Moreover, there are many reports about the increase in non-metallic enzyme activity in hybrid nanoflowers, such as lipase [35] and glucose oxidase [36]. DhaA is a non-metallic enzyme; thus, we expect that the immobilized enzyme prepared by suitable metal ions can improve its activity. Therefore, we investigated the effects of seven common metal ions as inorganic carriers on the activity recovery (AR) and encapsulation yield (EY) of immobilized DhaA. As shown in Figure 2, the EY of each metal-immobilized enzyme increased with the metal ion concentration, and the EY of  $\text{Co}^{2+}$ ,  $\text{Fe}^{3+}$ ,  $\text{Zn}^{2+}$  and  $\text{Al}^{3+}$  reached more than 80%. However, the AR was mostly reduced, which might be due to the inhibition of enzyme activity caused by the excessive concentration of metal ions [37]. The average AR of  $\text{Co}^{2+}$  and  $\text{Al}^{3+}$  hybrid nanocomposites could obtain about 60%. Surprisingly, the AR of  $\text{Fe}^{3+}$  hybrid nanocomposites could reach more than 90%, while the AR of other metal ions ( $\text{Cu}^{2+}$  for 18%,  $\text{Mn}^{3+}$  for 7%,  $\text{Ni}^{2+}$  for 19%, and  $\text{Zn}^{2+}$  for 15%) was seriously inhibited. Therefore, iron-based DhaA hybrid nanocomposites ( $\text{FeHN@DhaA}$ ) were selected as the research goal of this work.

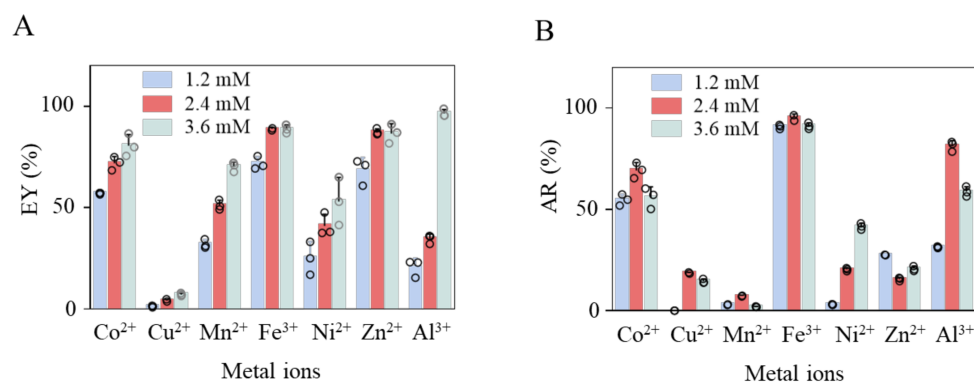


**Figure 2.** Effects of metal ions on EY (A) and AR (B) of immobilized enzymes.

### 2.2.2. The Effects of Enzyme Concentration

The effect of DhaA concentration (0.01–0.18 mg/mL) on the AR and EY of FeHN@DhaA was investigated (Figure 3A). With the increase in DhaA concentration, the AR of FeHN@DhaA increased at first and then decreased. When the enzyme concentration reached 0.07 mg/mL, the AR was  $106.38 \pm 1.15\%$ . In addition, with the elevation of DhaA concentration, the EY of FeHN@DhaA decreased gradually. The reason might be that the enzyme would act as a “glue” in the process of self-assembly, sticking the nanocrystals of metallophosphate together [25]. When the enzyme concentration was too low, the bonding effect was weak, which made the structure of nanoflowers loose and the enzyme loading of the whole immobilized system was minimal. When the enzyme concentration was relatively high, the crystal structure became very dense, and the whole system was in a state of overload [25]. The mass transfer efficiency in the reaction process was affected, and the AR decreased.

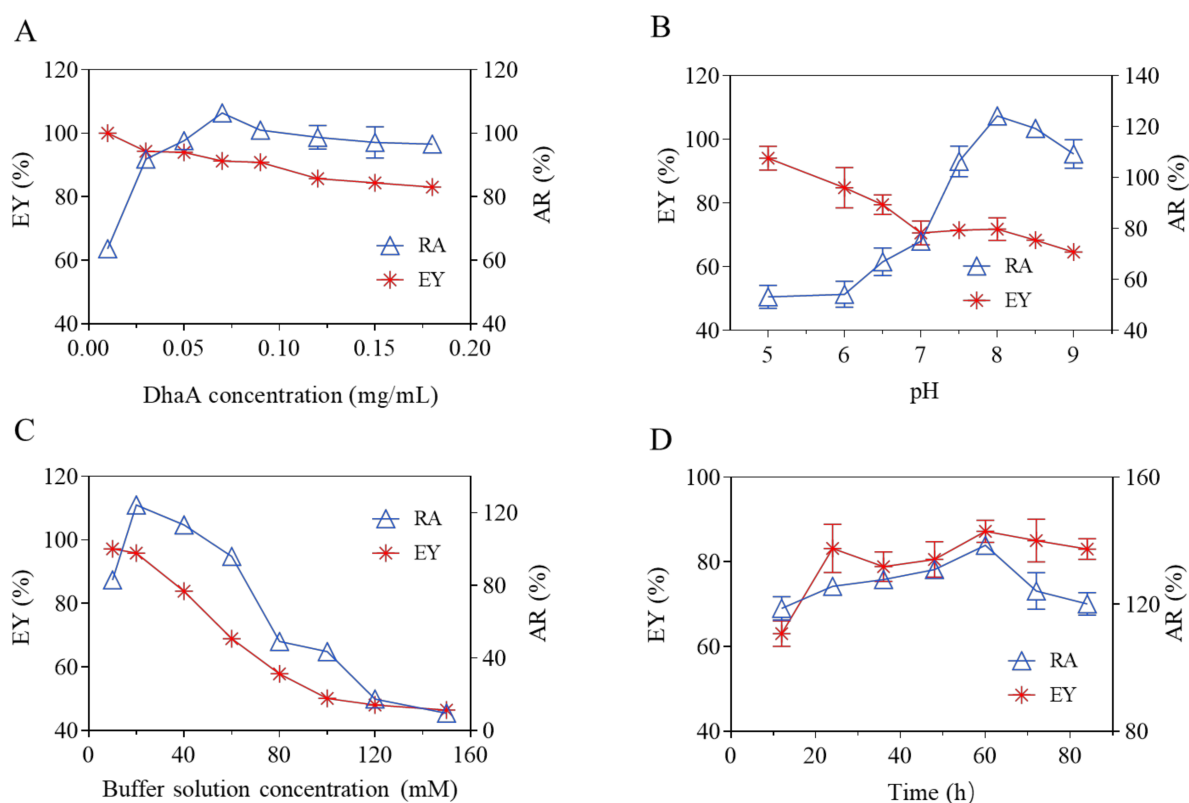


**Figure 3.** Synthetic process of immobilized enzyme. Effects of DhaA concentration (A), pH value (B), PB buffer concentration (C), and incubation time (D) on EY and AR of immobilized enzymes.

### 2.2.3. The Effects of pH

The different pH values will change the charge of the enzyme, thus affecting the interaction between the components in the immobilized synthesis system and the morphology and properties of the final product [38]. Therefore, we investigated the effect of the pH values from 5 to 9 on the preparation of FeHN@DhaA. As shown in Figure 3B, the AR and the effective EY of FeHN@DhaA were  $124.21 \pm 0.20\%$  and  $71.82 \pm 2.90\%$  after incubation at pH 8.0, respectively. However, the EY was  $94.11 \pm 3.05\%$  at pH 5.0, and the enzyme AR was only  $53.17 \pm 3.73\%$ . The possible reason is that in the case of low pH, protonation will make the enzyme positively charged, preventing the interaction between enzyme molecules and metal ions [39]. In the case of high pH, there is a strong repulsion between negatively charged enzyme molecules, which is also not conducive to the formation of metal hybrid nanoflowers [39].

#### 2.2.4. The Effects of PB Buffer Concentration

In order to explore whether the buffer concentration would affect the immobilization efficiency, the formation of FeHN@DhaA was evaluated in different concentrations of PB buffer. As illustrated in Figure 3C, the FeHN@DhaA synthesized with the concentration of PB buffer in 20 mM had the highest AR with  $124.20 \pm 0.25\%$ , and the EY was  $97.71 \pm 2.33\%$ . When the concentration of PB buffer was higher than 20 mM, the EY and AR showed a downward trend. This is consistent with the results reported by Ke et al., in which the immobilization effect of  $\text{Ca}_3(\text{PO}_4)_2$ -lipase hybrid nanoflowers in PB concentration 20 mM was the highest, and the relative activity was 308% compared to the free lipase [40]. Generally, the formation of a hybrid nanoflower structure is incomplete with a low concentration of PB when embedded with excess metal phosphate with a high PB concentration.

#### 2.2.5. The Effects of Incubation Time

In previous studies, it has been reported that the synthesis of hybrid nanoflowers experienced three steps: nucleation, condensation, and assembly into flower-like structures [22]. We investigated the effect of the incubation time (12–72 h) on the preparation of FeHN@DhaA. As shown in Figure 3D, the AR and the effective EY of FeHN@DhaA were  $124.19 \pm 4.68\%$  and  $85.02 \pm 4.14\%$  after incubation for 72 h, respectively. However, the synthesis of FeHN@DhaA showed better results ( $138.54 \pm 0.44\%$  and  $87.21 \pm 2.14\%$ ) when the incubation time was 60 h. Therefore, a reaction time that was too long also had an adverse effect on the AR. The nucleation of the metal phosphates and the in situ precipitation of the formed nanoparticles dominated the synthesizing proportion of enzymes in the hybrid nanoflowers significantly, thus destroying the enzymatic activity of the immobilized enzymes [24].

#### 2.3. Characterization of FeHN@DhaA

The prepared FeHN@DhaA was fully characterized by SEM, EDX, FT-IR and XRD to validate our design of immobilized DhaA. As shown in Figure 4A–C, the freeze-dried inorganic carrier, DhaA powders, and FeHN@DhaA were imaged via SEM in order to clearly illustrate the morphology of FeHN@DhaA. No significant hybrid nanostructures were detected among the DhaA powders or the inorganic carrier particles, while FeHN@DhaA exhibited granular nanostructures. The reason why it was different from the typical nanoflower structure may have been the cooperative influence of  $\text{Fe}^{3+}$  and the specific organic component DhaA. The dispersed nanoparticle structure of FeHN@DhaA increased the specific surface area, which may be the reason for the increase in enzyme activity after immobilization. In addition, the nucleation sites formed by metal ions in the protein region also affected the functional properties of the immobilized enzyme [41]. The fragment transformation method can predict the binding sites of metal and enzyme proteins based on the sequence and structural information contained in the target protein fragments [42]. Based on the structural information of DhaA, we used the method of fragment transformation to predict the potential nucleation sites for  $\text{Fe}^{3+}$  in the crystal structure of DhaA (PDB: 4E46) during mineralization. Figure 4D showed the metal binding residues according to the scoring criteria and selected the amino acids whose normalized scores were higher than 1.9. These values were higher than the threshold of the method, which ensured the prediction accuracy of the binding sites.

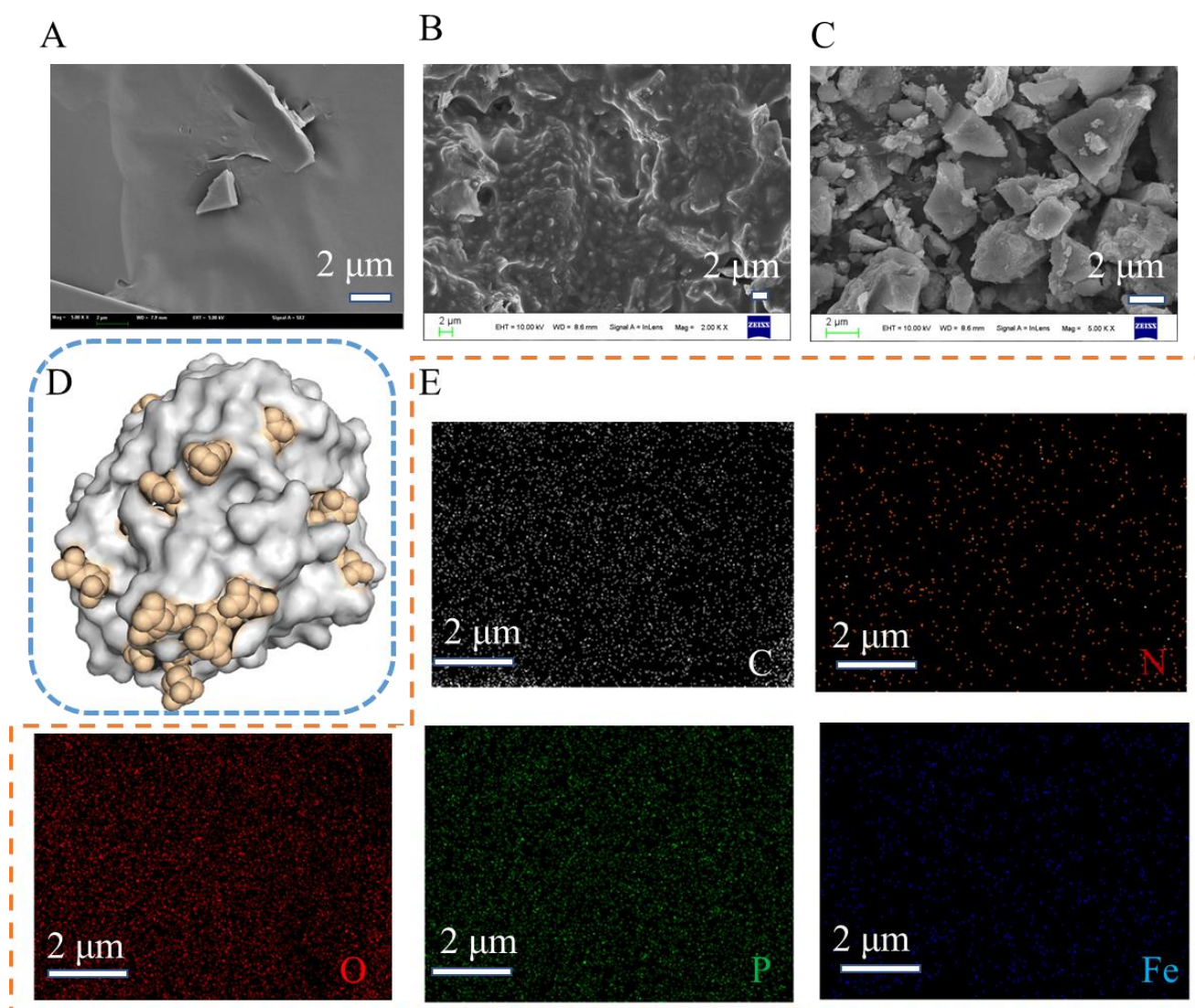


**Figure 4.** FE-SEM images of DhaA powder (A), inorganic carrier (B), and immobilized DhaA (C). Predicted residues involved in biomineral nucleation are presented as yellow spheres for  $\text{Fe}^{3+}$ ; the images were created using Pymol 2.2 (D). EDX elemental mapping of the immobilized DhaA (all elements, C, N, O, P, and Fe) (E).

EDX analysis was utilized to characterize FeHN@DhaA composition. As shown in Figure 4E, the presence of carbon (C) and nitrogen (N) was attributed to DhaA protein, and the existence of phosphorus (P) and iron (Fe) was due to the inorganic phosphate carriers. These results further confirm the successful preparation of DhaA–iron phosphate hybrid nanocomposites.

As shown in Figure 5A, FT-IR spectroscopy provided direct evidence for the formation of DhaA–inorganic hybrid nanocomposites. The FT-IR spectra of inorganic carriers and FeHN@DhaA showed the same diffraction peak at  $600\text{--}650\text{ cm}^{-1}$  and  $950\text{--}1100\text{ cm}^{-1}$ , such as P–O and O=P–O, which were assigned to the vibration of  $\text{PO}_4^{3-}$  (Figure 4B). The wide and strong band at  $2800\text{--}3000\text{ cm}^{-1}$  was attributed to  $-\text{CH}_2$  and  $-\text{CH}_3$ . The bands at  $950\text{--}1100\text{ cm}^{-1}$  and  $2800\text{--}3000\text{ cm}^{-1}$  were weakened after immobilization. More importantly, the characteristic peak of FeHN@DhaA at  $1540\text{ cm}^{-1}$  corresponded to the N–H bending vibrations (amide II band), which was not observed in the control inorganic carriers.

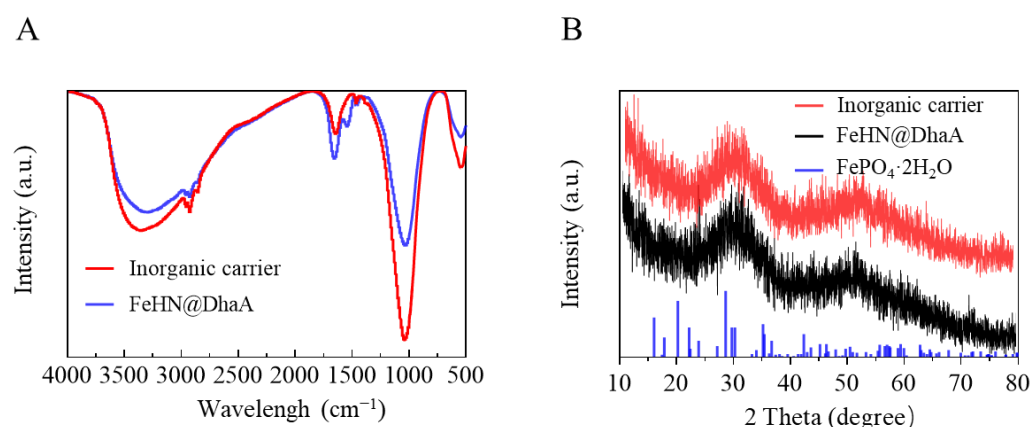


**Figure 5.** FT-IR spectra of inorganic carrier and immobilized DhaA (A); XRD patterns of inorganic carrier and immobilized DhaA (B).

In order to further investigate the crystal structure of FeHN@DhaA, XRD analysis was performed on the products in the range of 10–90°. The XRD pattern of the synthesized iron phosphate carriers and FeHN@DhaA is shown in Figure 5B. All the diffraction peaks in the XRD spectrum of FePO<sub>4</sub> were in good agreement with FePO<sub>4</sub>·2H<sub>2</sub>O, as indexed by the JCPDS X-ray powder diffraction file of No. 33-0667. This demonstrated that good crystallinities of FeHN@DhaA were formed, and the inorganic composition of FeHN@DhaA was FePO<sub>4</sub>·2H<sub>2</sub>O.

#### 2.4. Optimum Reaction Temperature and pH

The temperature and pH of the surrounding environment has significant effect on the activity of enzymes. In this study, bis (2-chloroethyl) ether was used as the substrate to determine the optimal reaction conditions. Figure 6A revealed the temperature profiles of the free and immobilized DhaA. There was no difference in the optimum temperature between the free and immobilized DhaA: both were 40 °C. In addition, the relative activity of the immobilized enzyme FeHN@DhaA was always higher than that of the free enzyme, especially at 20–40 °C. Similarly, FeHN@DhaA maintained higher enzyme activity than free DhaA in the pH range of 6.0–9.5 (Figure 6B). It is worth noting that the relative activity of FeHN@DhaA was always 1.4–2-fold higher than that of free enzymes in the pH range of 6.0–8.0. Overall, the wider temperature and pH range of immobilized enzymes could be attributed to the chelating effect between DhaA molecules and metal phosphate nanoparticles, which enhance the rigidity of DhaA and prevent the denaturation of proteins under extreme conditions, as described previously [43]. Therefore, the excellent performance of the immobilized enzyme FeHN@DhaA shows that it could be a promising candidate for the decontamination of organochlorine pesticides in the environment (industrial effluent).

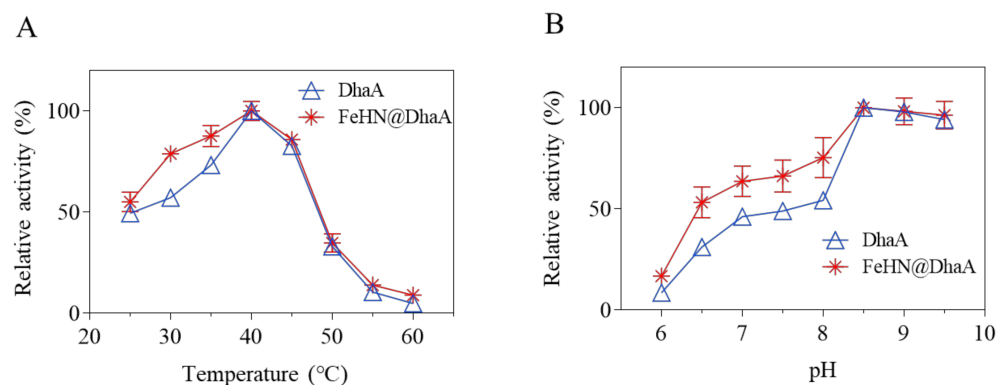


**Figure 6.** Optimum temperature (A) and pH (B) of free and immobilized DhaA.

### 2.5. Stability and Reusability of FeHN@DhaA

The stability and reusability of biocatalysts in relation to environmental factors are important indicators to evaluate their practical application [44]. In this work, the stability of FeHN@DhaA in relation to temperature, pH and storage properties was investigated and the reusability of FeHN@DhaA was further explored with five consecutive reactions.

As shown in Figure 7A, a thermal stability test was conducted at different temperatures. As can be seen, the relative activity of FeHN@DhaA was obviously higher than that of the free enzyme from 20 °C to 35 °C. The relative activity of the immobilized enzyme decreased after more than 40 °C. The reason for the poor thermal stability of the immobilized enzyme might be due to the trivalent iron-based hybrid nanocomposites, which are different from the divalent metal ions selected by most hybrid nanoflowers as the inorganic components. The stability of FeHN@DhaA was 1.4-fold higher than that of the free enzyme at 40 °C (optimum reaction temperature), which indicated that it still has some practical application potential. In fact, the catalytic reaction of FeHN@DhaA was an acid-producing reaction, and improving its acidic stability was of more significance for the enzymatic reaction. As shown in Figure 7B, the relative activity of FeHN@DhaA was maintained at more than 50% in the range of pH 4.0–9.0. In addition, the relative activity of the immobilized enzyme FeHN@DhaA in the range of pH 4.0–5.0 was always twice as high as that of the free enzyme. Therefore, the resistance of FeHN@DhaA to acidic conditions was more suitable for the actual catalytic reaction process of DhaA. Compared with the previously reported immobilized DhaA [15,18], FeHN@DhaA showed stronger pH stability. A possible explanation is that phosphate can confine the enzyme in the nanostructure, resulting in the increased rigidity of the enzyme to cope with conformational changes and avoid the inactivation and denaturation of the enzyme in an adverse environment [45].

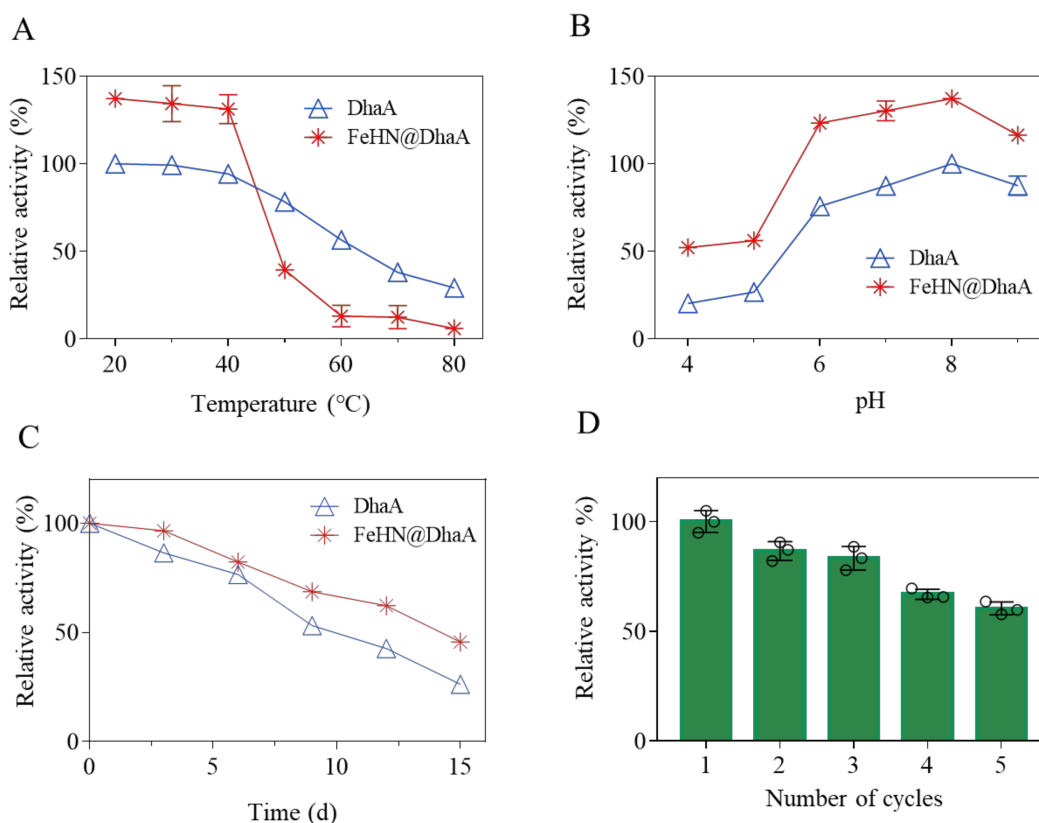


**Figure 7.** Thermal (A), pH (B) and long-term storage (C) stability of free and immobilized DhaA. Reusability of immobilized DhaA (D).

To examine the prepared FeHN@DhaA in terms of superiority, the residual enzyme activity was determined under standard assay conditions. As shown in Figure 7C, the relative activity of the free enzyme was  $26.25 \pm 0.16\%$  after storage for half a month at room temperature. However, the immobilized enzyme FeHN@DhaA still remained at  $45.6 \pm 1.23\%$  of its initial activity under the same conditions. These results clearly demonstrate that the immobilization of DhaA into iron phosphate hybrid nanocomposites improves storage stability and has great potential in industrial application. Hence, the reusability performance of FeHN@DhaA was assessed by five consecutive cycles. As shown in Figure 7D, relative activity gradually decreased with an increasing number of cycles. However, even in the fifth cycle, FeHN@DhaA retained a relative activity of  $57.85 \pm 2.42\%$ . The gradual and insignificant decline in relative activity may be due to the partial FeHN@DhaA deformation and deactivation during the reaction with the substrate, and/or the partial leakage of the biocatalyst during continuous washing and separating operations [44,46]. Reusability is one of the essential advantages of immobilized DhaA compared with the free form, as this can reduce cost in practical applications.

### 3. Materials and Methods

#### 3.1. Materials

Bis (2-chloroethyl) ether was purchased from Shanghai Pesticide Research Center ( $\text{Na}_2\text{HPO}_4$ ,  $\text{NaH}_2\text{PO}_4$ ,  $\text{CuSO}_4$ ,  $\text{CoSO}_4$ ,  $\text{MnSO}_4$ , and  $\text{Fe}_2(\text{SO}_4)_3$ ). All the other reagents (analytical grade) were purchased from Sinopharm Chemical Reagent Co., Ltd. (Shanghai, China). Mercuric thiocyanate and ferric ammonium sulfate were obtained from the Research Institute of Chemical Defense (Beijing, China).

#### 3.2. Purification of Recombinant DhaA

Recombinant *E. coli* BL21 (DE3) harboring the pET28a-DhaA construct was cultured in 40 mL terrific broth (TB) medium containing kanamycin at  $37^\circ\text{C}$ . The strain was incubated at  $37^\circ\text{C}$  with 200 rpm until the optical density (OD) was achieved 1.8 at 600 nm (MAPADA, UV-3200, Shanghai, China), followed by incubation with 0.4 mM isopropylthio- $\beta$ -galactoside (IPTG) at  $20^\circ\text{C}$  with shaking at 200 rpm for 22 h. The cells were harvested through centrifugation at 12,000 rpm for 20 min at  $4^\circ\text{C}$ . The cells were then lysed by sonication and centrifuged again at 12,000 rpm for 10 min to separate soluble from insoluble proteins. Purification was accomplished using 5 mL HisTrap FF affinity column (GE Healthcare). The column was equilibrated with a buffer A (25 mM Tris, 20 mM imidazole, and 500 mM NaCl, pH 7.4) and then loaded with the crude enzyme buffered at pH 7.4. The column was washed with buffer A of up to 5 column volumes to wash out any unbound protein. The purified protein was then eluted using linear gradient (20–500 mM imidazole) elution with buffer B (20 mM Tris, 500 mM imidazole and 500 mM NaCl, pH 7.4). The eluted sample was further used for SDS-PAGE (10%) and activity analysis. The purified enzymes were then stored at  $4^\circ\text{C}$  for use in further experiments.

#### 3.3. Enzymatic Activity Assay

The enzymatic activities of the free and immobilized DhaA samples were measured by a modified colorimetric assay [14]. In brief, 10 mM bis (2-chloroethyl) ether was incubated with the free and immobilized DhaA samples in 0.1 mM Gly-NaOH buffer (pH 8.0) at  $40^\circ\text{C}$  for 20 min. The reaction was arrested by the addition of 30% (*v/v*) nitric acid (20  $\mu\text{L}$ ) to 200  $\mu\text{L}$  of the reaction system, followed by the addition of 55  $\mu\text{L}$  of mercuric thiocyanate and 110  $\mu\text{L}$  of ferric ammonium sulfate. After mixing and standing for 10 min, 200  $\mu\text{L}$  was added to the 96-well plate, and the absorbance at 460 nm was measured by an enzyme labeling instrument. One unit of enzyme activity was defined as the amount of the enzyme that could release 1  $\mu\text{mol}$  of chloride ion per minute. The calculation formula for the specific activity of DhaA was as follows:

$$S = \frac{CV}{TM} \quad (1)$$

where  $S$  (U/mg) is the specific activity of DhaA,  $C$  ( $\mu\text{M}$ ) is the concentration of chloride ion,  $V$  (L) is the total volume of the mixture,  $T$  (min) is the reaction time, and  $M$  (mg) is the total mass of the enzyme.

#### 3.4. Preparation of Metal–DhaA Hybrid Nanocomposites

The hybrid nanocomposites were synthesized as previously described with some modifications [22]. Briefly, 0.01–0.18 mg/mL DhaA samples were mixed with 1.2–3.6 mM metal salt solution in 2 mL phosphate buffer (PB, 10–120 mM, pH 5.0–9.0) to optimize the condition for the synthesis of hybrid nanocomposites. After gently shaking for 5 min, the sample was further incubated at 4 °C for 12–72 h. Subsequently, the prepared hybrid nanocomposites were collected by centrifugation at 10,000 rpm for 10 min and washed three times with deionized water.

The encapsulation yield (EY) of DhaA in the hybrid nanocomposites was investigated using the Bradford assay method. The EY was calculated according to the following equation:

$$\text{EY} = \frac{\text{Immobilized amount of DhaA}}{\text{Total amount of DhaA used}} \times 100\% \quad (2)$$

In addition, the activity recovery (AR) test of the hybrid nanocomposites was also carried out and calculated as follows:

$$\text{AR} = \frac{\text{overall specific activity of immobilized DhaA}}{\text{initial specific activity of free DhaA}} \times 100\% \quad (3)$$

#### 3.5. Characterization of Metal–DhaA Hybrid Nanocomposites

Scanning electron microscopy (SEM), energy dispersive X-ray (EDX) analysis and mapping were performed on a JSM-7800F instrument to scan the hybrid nanocomposites to identify the surface morphology and analyze the structure under accelerating voltage 3 kV. The freeze-dried inorganic carrier and DhaA powders were used as references. The crystal structure of the hybrid nanocomposites was analyzed using X-ray diffraction (XRD, D2 PHASER, Brook AXS Ltd., Berlin, Germany) with a light pipe power of 2.2 kW, a scan range of 10–90°, and a scan step width of 0.2 for the Cu target. The free DhaA powders and hybrid nanocomposites were ground to 200 mesh before detection. Fourier infrared spectroscopy (FT-IR) was employed to identify significant functional group peaks. The measurements were obtained by using the KBr pressed-pellet method. Each sample was scanned at a range of 4000–400  $\text{cm}^{-1}$  wavenumbers.

#### 3.6. Effects of pH and Temperature

The effects of pH and temperature on free and immobilized DhaA were evaluated by measuring the activity in different pH values (pH 6.0–9.5) and different temperatures (25–60 °C). The activity detection method was described above, taking the maximum activity as 100%. By testing the EY, the content of free and immobilized DhaA was consistent. Thermal stabilities of free and immobilized DhaA were studied by measuring the residual activities of the DhaA after incubation at 20–80 °C for 40 min. pH stabilities of free and immobilized DhaA were evaluated by measuring the residual activities of the DhaA after incubation at pH value from 4.0 to 9.0 for 40 min. The determination method of enzyme activity after incubation was as described above, taking the maximum activity of free DhaA as 100%.

#### 3.7. Storage Stability and Reusability of Free and Immobilized DhaA

The determination of storage stability was that the free enzyme and immobilized enzyme were incubated at room temperature for 3 weeks. The same amount of samples were taken out every 3 days to determine the residual enzyme activity. The residual activities of the resultant samples were assayed as described above. The activity of the DhaA samples at day 0 was set as 100%. To test the reusability of the immobilized DhaA, the catalytic

reaction was repeated for five cycles. After one reaction, the hybrid nanocomposites were separated from the reaction mixture by centrifugation (10,000 rpm, 5 min) and washed three times with deionized water. The recovered hybrid nanocomposites were immediately used for the next reaction measurement. The absorption of the supernatant at 460 nm for the first measurement was set as 100%.

### 3.8. Statistical Analysis

All data in our experiments were derived from three parallel experiments and the average and standard deviation of the replicates were calculated. Statistical significance was determined by an analysis of variance (ANOVA) using Prism 5 (GraphPad Software Inc., San Diego, CA, USA). All experimental values are presented as mean values  $\pm$  standard deviations. The value of  $p < 0.05$  was considered as a significant difference.

## 4. Conclusions

To sum up, by adjusting the synthesis conditions, we developed an innovative biocatalyst with iron-based DhaA hybrid nanocomposites through a simple and green biomineralization approach. Based on organic–inorganic hybrid technology, the immobilized DhaA could effectively increase the enzyme activity of DhaA. FeHN@DhaA showed an effective encapsulation yield and activity recovery of and 87.21% and 138.54%, respectively. Compared with the free DhaA, FeHN@DhaA had a wider temperature and pH application range. Moreover, the storage stability of FeHN@DhaA at room temperature was significantly higher ( $p < 0.05$ ) than that of the free enzyme. More importantly, the immobilized enzyme exhibited efficient reusability by retaining 57.85% of relative activity in the fifth reaction cycle. Therefore, this activity-enhanced immobilized DhaA can be considered as a potentially useful tool in practical applications for the cleaning of halogenated compounds in contaminated soil, water and other environments.

**Author Contributions:** Conceptualization, J. and X.M.; methodology, Y.X.; software, Z.G. (Zitao Guo); validation, Y.S., M.L. and Z.G. (Zhongpeng Guo); formal analysis, Z.G. (Zhenghua Gu); investigation, Z.G. (Zhenghua Gu); resources, L.Z.; data curation, X.M.; writing—original draft preparation, J.C.; writing—review and editing, X.M.; visualization, X.G.; supervision, L.Z.; project administration, L.Z.; funding acquisition, L.Z. All authors have read and agreed to the published version of the manuscript.

**Funding:** This work was supported by the National Key Research & Developmental Program of China (2021YFC2100300); Beijing Nova Program (Z201100006820035); National Natural Science Foundation of China (81902071).

**Data Availability Statement:** The data for the current study are available from the corresponding author on request.

**Conflicts of Interest:** The authors declare no conflict of interest.

## References

1. Janssen, D.B. Evolving haloalkane dehalogenases. *Curr. Opin. Chem. Biol.* **2004**, *8*, 150–159. [[CrossRef](#)]
2. Keuning, S.; Janssen, D.B.; Witholt, B. Purification and Characterization of Hydrolytic Haloalkane Dehalogenase from *Xanthobacter autotrophicus* GJ10. *J. Bacteriol.* **1985**, *163*, 635–639. [[CrossRef](#)] [[PubMed](#)]
3. Kunka, A.; Damborsky, J.; Prokop, Z. Haloalkane Dehalogenases from Marine Organisms. *Methods Enzymol.* **2018**, *605*, 203–251. [[PubMed](#)]
4. Koudelakova, T.; Chovancova, E.; Brezovsky, J.; Monincova, M.; Fortova, A.; Jarkovsky, J.; Damborsky, J. Substrate specificity of haloalkane dehalogenases. *Biochem. J.* **2011**, *435*, 345–354. [[CrossRef](#)] [[PubMed](#)]
5. Nagata, Y.; Ohtsubo, Y.; Tsuda, M. Properties and biotechnological applications of natural and engineered haloalkane dehalogenases. *Appl. Microbiol. Biotechnol.* **2015**, *99*, 9865–9881. [[CrossRef](#)]
6. Koudelakova, T.; Bidmanova, S.; Dvorak, P.; Pavelka, A.; Chaloupkova, R.; Prokop, Z.; Damborsky, J. Haloalkane dehalogenases: Biotechnological applications. *Biotechnol. J.* **2012**, *8*, 32–45. [[CrossRef](#)]
7. Swanson, P.E. Dehalogenases applied to industrial-scale biocatalysis. *Curr. Opin. Biotechnol.* **1999**, *10*, 365–369. [[CrossRef](#)]
8. Quintero, J.C.; Moreira, M.T.; Feijoo, G.; Lema, J.M. Anaerobic degradation of hexachlorocyclohexane isomers in liquid and soil slurry systems. *Chemosphere* **2005**, *61*, 528–536. [[CrossRef](#)]

9. Oakley, A.; Prokop, Z.; Boháč, M.; Kmuniček, J.; Jedlička, T.; Monincová, M.; Kutá-Smatanová, I.; Nagata, Y.; Damborský, J.; Wilce, M. Exploring the structure and activity of haloalkane dehalogenase from *Sphingomonas paucimobilis* UT26: Evidence for product- and water-mediated inhibition. *Biochemistry* **2002**, *41*, 4847–4855. [[CrossRef](#)]
10. Bidmanova, S.; Chaloupkova, R.; Damborsky, J.; Prokop, Z. Development of an enzymatic fiber-optic biosensor for detection of halogenated hydrocarbons. *Anal. Bioanal. Chem.* **2010**, *398*, 1891–1898. [[CrossRef](#)]
11. Los, G.V.; Encell, L.P.; McDougall, M.G.; Hartzell, D.D.; Karassina, N.; Zimprich, C.; Wood, M.G.; Learish, R.; Ohana, R.F.; Urh, M. HaloTag: A Novel Protein Labeling Technology for Cell Imaging and Protein Analysis. *ACS Chem. Biol.* **2008**, *3*, 373–382. [[CrossRef](#)]
12. Pavlova, M.; Klvana, M.; Prokop, Z.; Chaloupkova, R.; Banas, P.; Otyepka, M.; Wade, R.C.; Tsuda, M.; Nagata, Y.; Damborsky, J. Redesigning dehalogenase access tunnels as a strategy for degrading an anthropogenic substrate. *Nat. Chem. Biol.* **2009**, *5*, 727–733. [[CrossRef](#)]
13. Zou, S.; Gu, K.; Zheng, Y. Covalent immobilization of haloalcohol dehalogenase for efficient synthesis of epichlorohydrin in an integrated bioreactor. *Biotechnol. Prog.* **2018**, *34*, 784–792. [[CrossRef](#)]
14. Zheng, H.; Yu, W.L.; Guo, X.; Zhao, Y.Z.; Cui, Y.; Hu, T.; Zhong, J.Y. An effective immobilized haloalkane dehalogenase DhaA from *Rhodococcus rhodochrous* by adsorption, crosslink and PEGylation on meso-cellular foam. *Int. J. Biol. Macromol.* **2019**, *125*, 1016–1023. [[CrossRef](#)]
15. Wang, M.; Yu, W.; Shen, L.; Zheng, H.; Hu, T. Conjugation of haloalkane dehalogenase DhaA with arabinogalactan to increase its stability. *J. Biotechnol.* **2021**, *335*, 47–54. [[CrossRef](#)]
16. Shan, Y.; Yu, W.; Shen, L.; Guo, X.G.; Han, Y. Conjugation with inulin improves the environmental stability of haloalkane dehalogenase DhaA. *Enzym. Microb. Technol.* **2021**, *149*, 109832. [[CrossRef](#)]
17. Zheng, H.; Zhong, J.Y.; Cui, Y.; Zhang, Z.; Zhao, C.L.; Zhao, Y.Z.; Zheng, Y.C.; Guo, X. Mesoporous support designed for DhaA adsorption with improved stability. *J. Porous Mater.* **2019**, *26*, 829–837. [[CrossRef](#)]
18. Zhang, X.J.; Shi, P.X.; Deng, H.Z.; Wang, X.X.; Liu, Z.Q.; Zheng, Y.G. Biosynthesis of chiral epichlorohydrin using an immobilized haloalcohol dehalogenase in aqueous and non-aqueous phase. *Bioresour. Technol.* **2018**, *263*, 483–490. [[CrossRef](#)]
19. Ding, S.; Cargill, A.A.; Medintz, I.L.; Claussen, J.C. Increasing the activity of immobilized enzymes with nanoparticle conjugation. *Curr. Opin. Biotechnol.* **2015**, *34*, 242–250. [[CrossRef](#)]
20. Luckarift, H.R.; Spain, J.C.; Naik, R.R.; Stone, M.O. Enzyme immobilization in a biomimetic silica support. *Nat. Biotechnol.* **2004**, *22*, 211–213. [[CrossRef](#)]
21. An, J.; Li, G.; Zhang, Y.; Zhang, T.; Fan, H. Recent Advances in Enzyme-Nanostructure Biocatalysts with Enhanced Activity. *Catalysts* **2020**, *10*, 338. [[CrossRef](#)]
22. Ge, J.; Lei, J.; Zare, R.N. Protein–inorganic hybrid nanoflowers. *Nat. Nanotechnol.* **2012**, *7*, 428–432. [[CrossRef](#)]
23. Cui, J.; Jia, S. Organic–inorganic hybrid nanoflowers: A novel host platform for immobilizing biomolecules. *Coord. Chem. Rev.* **2017**, *352*, 249–263. [[CrossRef](#)]
24. Li, Y.; Wu, H.; Su, Z. Enzyme-based hybrid nanoflowers with high performances for biocatalytic, biomedical, and environmental applications. *Coord. Chem. Rev.* **2020**, *416*, 213342. [[CrossRef](#)]
25. Zhang, M.; Zhang, Y.; Yang, C.; Ma, C.; Tang, J. Enzyme-inorganic hybrid nanoflowers: Classification, synthesis, functionalization and potential applications. *Chem. Eng. J.* **2021**, *415*, 129075. [[CrossRef](#)]
26. Dube, S.; Rawtani, D. Understanding intricacies of bioinspired organic-inorganic hybrid nanoflowers: A quest to achieve enhanced biomolecules immobilization for biocatalytic, biosensing and bioremediation applications. *Adv. Colloid Interface Sci.* **2021**, *295*, 102484. [[CrossRef](#)]
27. Wei, J.; Wang, X.; Yang, J.; Han, H.; Tang, J. Lipase-inorganic hybrid nanoflower constructed through biomimetic mineralization: A new support for biodiesel synthesis. *J. Colloid Interface Sci.* **2018**, *514*, 102–107.
28. Hu, R.; Zhang, X.; Zhao, Z.; Zhu, G.; Chen, T.; Fu, T.; Tan, W. DNA nanoflowers for multiplexed cellular imaging and traceable targeted drug delivery. *Angew. Chem. Int. Ed. Engl.* **2014**, *53*, 5821–5826. [[CrossRef](#)]
29. Rong, J.; Zhang, T.; Qiu, F.; Zhu, Y. Preparation of Efficient, Stable, and Reusable Laccase–Cu<sub>3</sub>(PO<sub>4</sub>)<sub>2</sub> Hybrid Microspheres Based on Copper Foil for Decoloration of Congo Red. *ACS Sustain. Chem. Eng.* **2017**, *5*, 4468–4477. [[CrossRef](#)]
30. Fu, M.; Xing, J.; Ge, Z. Preparation of laccase-loaded magnetic nanoflowers and their recycling for efficient degradation of bisphenol A. *Sci. Total Environ.* **2018**, *651*, 2857–2865. [[CrossRef](#)]
31. Lin, Z.; Xiao, Y.; Yin, Y.; Hu, W.; Liu, W.; Yang, H. Facile Synthesis of Enzyme-Inorganic Hybrid Nanoflowers and Its Application as a Colorimetric Platform for Visual Detection of Hydrogen Peroxide and Phenol. *ACS Appl. Mater. Interfaces* **2012**, *6*, 10775–10782. [[CrossRef](#)] [[PubMed](#)]
32. Wang, L.B.; Wang, Y.C.; He, R.; Zhuang, A.; Wang, X.; Jie, Z.; Hou, J.G. A new nanobiocatalytic system based on allosteric effect with dramatically enhanced enzymatic performance. *J. Am. Chem. Soc.* **2013**, *135*, 1272. [[CrossRef](#)] [[PubMed](#)]
33. Somturk, B.; Yilmaz, I.; Altinkaynak, C.; Karatepe, A.; Özdemir, N.; Ocoy, I. Synthesis of urease hybrid nanoflowers and their enhanced catalytic properties. *Enzym. Microb. Technol.* **2016**, *86*, 134–142. [[CrossRef](#)] [[PubMed](#)]
34. Chen, J.; Guo, Z.; Zhang, H.; Xin, Y.; Shi, Y.; Gu, Z.; Zhang, L.; Zhong, J.; Guo, X.; Li, Y.; et al. Development of a multimetal-based phosphotriesterase hybrid nanoflowers for decontamination of environmental organophosphorus compounds pollution. *Chem. Eng. J.* **2022**, *446*, 136933. [[CrossRef](#)]

35. Cui, J.; Zhao, Y.; Liu, R.; Cheng, Z.; Jia, S. Surfactant-activated lipase hybrid nanoflowers with enhanced enzymatic performance. *Sci. Rep.* **2016**, *6*, 27928. [[CrossRef](#)]
36. Batule, B.S.; Park, K.S.; Gautam, S.; Cheon, H.J.; Kim, M.I.; Park, H.G. Intrinsic peroxidase-like activity of sonochemically synthesized protein copper nanoflowers and its application for the sensitive detection of glucose. *Sens. Actuators B Chem.* **2019**, *283*, 749–754. [[CrossRef](#)]
37. Hao, M.; Fan, G.; Zhang, Y.; Xin, Y.; Zhang, L. Preparation and characterization of copper-Brevibacterium cholesterol oxidase hybrid nanoflowers. *Int. J. Biol. Macromol.* **2019**, *126*, 539–548. [[CrossRef](#)]
38. Ocoy, I.; Somturk, B.; Hancer, M.; Özdemir, N. Synthesis of copper ion incorporated horseradish peroxidase-based hybrid nanoflowers for enhanced catalytic activity and stability. *Dalton Trans.* **2015**, *44*, 13845–13852.
39. Nadar, S.S.; Gawas, S.D.; Rathod, V.K. Self-assembled organic-inorganic hybrid glucoamylase nanoflowers with enhanced activity and stability. *Int. J. Biol. Macromol.* **2016**, *92*, 660–669. [[CrossRef](#)]
40. Ke, C.; Fan, Y.; Chen, Y.; Xu, L.; Yan, Y. A new lipase–inorganic hybrid nanoflower with enhanced enzyme activity. *RSC Adv.* **2016**, *6*, 19413–19416. [[CrossRef](#)]
41. Mesa, M.; Velasco-Lozano, S.; Bernal, C.; Lin, Y.-F.; Escobar, S. Understanding the functional properties of bio-inorganic nanoflowers as biocatalysts by deciphering the metal-binding sites of enzymes. *J. Mater. Chem. B Mater. Biol. Med.* **2017**, *5*, 4478–4486. [[CrossRef](#)]
42. Lin, Y.F.; Cheng, C.W.; Shih, C.S.; Hwang, J.K.; Yu, C.S.; Lu, C.H. MIB: Metal Ion-Binding Site Prediction and Docking Server. *J. Chem. Inf. Modeling* **2016**, *56*, 2287–2291. [[CrossRef](#)]
43. Li, Z.; Chen, Z.; Zhu, Q.; Song, J.; Liu, X. Improved performance of immobilized laccase on Fe<sub>3</sub>O<sub>4</sub>@C-Cu<sup>2+</sup> nanoparticles and its application for biodegradation of dyes. *J. Hazard. Mater.* **2020**, *399*, 123088. [[CrossRef](#)]
44. Chen, Z.; Yao, J.; Šolević Knudsen, T.; Ma, B.; Liu, B.; Li, H.; Zhu, X.; Zhao, C.; Pang, W.; Cao, Y. Degradation of novel mineral flotation reagent 8-hydroxyquinoline by superparamagnetic immobilized laccase: Effect, mechanism and toxicity evaluation. *Chem. Eng. J.* **2022**, *432*, 134239. [[CrossRef](#)]
45. Chen, J.; Guo, Z.; Xin, Y.; Shi, Y.; Zhang, L. Preparation of efficient, stable, and reusable copper-phosphotriesterase hybrid nanoflowers for biodegradation of organophosphorus pesticides. *Enzym. Microb. Technol.* **2021**, *146*, 109766. [[CrossRef](#)]
46. Wu, J.; Ma, X.; Li, C.; Zhou, X.; Han, J.; Wang, L.; Dong, H.; Wang, Y. A novel photon-enzyme cascade catalysis system based on hybrid HRP-CN/Cu<sub>3</sub>(PO<sub>4</sub>)<sub>2</sub> nanoflowers for degradation of BPA in water. *Chem. Eng. J.* **2022**, *427*, 131808. [[CrossRef](#)]